






Geochemistry, Geophysics, Geosystems®



RESEARCH ARTICLE

10.1029/2023GC011379

Molybdenum Isotope Fingerprinting of Microbial Sulfate Reduction in Seep Carbonate Rocks

Zice Jia^{1,2}, Yu Hu¹ , Germain Bayon³, Jörn Peckmann⁴ , Xudong Wang¹, Shanggui Gong¹, Jie Li⁵ , Harry H. Roberts⁶, Duofu Chen^{1,2} , and Dong Feng^{1,2} 

Key Points:

- Organic matter tends to adsorb isotopically light Mo, resulting in low $\delta^{98}\text{Mo}$ values of organic matter in marine environments
- Isotopically light Mo is inferred to be preferentially adsorbed onto organic matter during enhanced sulfate reduction
- $\delta^{98}\text{Mo}$ offset between carbonate and organic phases in authigenic carbonates is promising to trace the past intensity of sulfate reduction

Correspondence to:

Y. Hu and D. Feng,
huyu@shou.edu.cn;
dfeng@shou.edu.cn

Citation:

Jia, Z., Hu, Y., Bayon, G., Peckmann, J., Wang, X., Gong, S., et al. (2024). Molybdenum isotope fingerprinting of microbial sulfate reduction in seep carbonate rocks. *Geochemistry, Geophysics, Geosystems*, 25, e2023GC011379. <https://doi.org/10.1029/2023GC011379>

Received 7 DEC 2023

Accepted 20 FEB 2024

¹College of Oceanography and Ecological Science, Shanghai Ocean University, Shanghai, China, ²Laboratory for Marine Mineral Resources, Qingdao National Laboratory for Marine Science and Technology, Qingdao, China, ³University Brest, CNRS, Ifremer, Geo-Ocean, Plouzané, France, ⁴Center for Earth System Research and Sustainability, Institute for Geology, Universität Hamburg, Hamburg, Germany, ⁵State Key Laboratory of Isotope Geochemistry, Guangzhou Institute of Geochemistry, Chinese Academy of Sciences, Guangzhou, China, ⁶College of the Coastal and Environment, Coastal Studies Institute, Louisiana State University, Baton Rouge, LA, USA

Abstract Understanding the interaction between molybdenum (Mo) and organic matter during microbial sulfate reduction is critical for the use of Mo to reconstruct marine redox conditions throughout Earth's history. However, little is known about Mo isotope fractionation and how it relates to organic matter remineralization during microbial sulfate reduction. Here, we report Mo abundances and isotopic ($\delta^{98}\text{Mo}$) compositions for bulk-rock, non-lithogenic and sequentially extracted fractions, including carbonate (*carb*), pyrite, and organic matter (*OM*), of seep carbonate rocks. Our data indicate that the difference between $\delta^{98}\text{Mo}_{\text{carb}}$ and $\delta^{98}\text{Mo}_{\text{OM}}$ ($\Delta^{98}\text{Mo}_{\text{carb-OM}}$) displays significant variability in the studied samples, ranging between 0.72 and 1.01‰. Remarkably, the obtained $\Delta^{98}\text{Mo}_{\text{carb-OM}}$ values indicate correlative trends with stable carbon isotope ratios and bulk abundances of (a) total organic carbon, (b) Mo, and (c) pyrite in seep carbonates, which we interpret as reflecting sustained adsorption of isotopically light Mo onto organic matter during enhanced sulfate reduction. On this basis, we put forward the concept that $\Delta^{98}\text{Mo}_{\text{carb-OM}}$ of authigenic carbonate rocks can be used as a measure of the intensity of sulfate reduction and for reconstructing past interactions between Mo and organic matter in marine sediments.

Plain Language Summary Molybdenum (Mo) is a useful element for reconstructing marine redox conditions throughout the Earth's history. The sequestration of Mo through sulfate-reducing bacterial activity acts as a significant pathway for Mo burial in the ocean. However, the impact of microbial sulfate reduction in Mo isotope fractionation remains unclear, preventing the understanding of the interaction between Mo and organic matter. We report Mo abundances and isotopic ($\delta^{98}\text{Mo}$) compositions for different phases extracted from seep carbonate rock fractions, including carbonate (*carb*), pyrite, and organic matter (*OM*). Our findings indicate that organic matter tends to preferentially adsorb isotopically light Mo. The observed $\delta^{98}\text{Mo}$ difference between carbonate and organic matter fractions ($\Delta^{98}\text{Mo}_{\text{carb-OM}}$ from 0.72 to 1.01‰) represents the first report of the extent of Mo isotope fractionation during Mo adsorption to organic matter in marine environments. We attribute greater $\Delta^{98}\text{Mo}_{\text{carb-OM}}$ offsets to the preferential adsorption of isotopically light Mo onto organic matter during enhanced sulfate reduction, and in turn put forward the idea that such offsets can be possibly used in the sedimentary record to trace the intensity of sulfate reduction and to reconstruct the past interaction between Mo and organic matter in marine sediments.

1. Introduction

Over the past decades, molybdenum isotopes ($\delta^{98}\text{Mo}$) have been widely used to explore the history of oceanic redox conditions (e.g., Arnold et al., 2004; Chen et al., 2015; Cheng et al., 2020; Dickson, 2017; Dickson et al., 2014; Goldberg et al., 2016; O'Sullivan et al., 2022). As a redox sensitive trace metal, Mo is highly soluble in oxic seawater and has a long residence time of ca. 440 ka (Colodner et al., 1995; Emerson & Husted, 1991; Miller et al., 2011). Dissolved Mo has a strong affinity to iron (Fe) and manganese (Mn) oxides under oxic conditions, leading to the preferential adsorption of isotopically light Mo onto Fe-Mn oxides with a maximum fractionation factor up to 3‰ relative to the ambient value (e.g., Barling & Anbar, 2004; Barling et al., 2001; Chen et al., 2022; Eroglu et al., 2020; Goldberg et al., 2009; Scholz et al., 2017; Siebert et al., 2003; Wasylenki et al., 2008). In environments characterized by low concentrations of dissolved hydrogen sulfide with

© 2024 The Authors. *Geochemistry, Geophysics, Geosystems* published by Wiley Periodicals LLC on behalf of American Geophysical Union. This is an open access article under the terms of the [Creative Commons Attribution-NonCommercial-NoDerivs License](https://creativecommons.org/licenses/by/4.0/), which permits use and distribution in any medium, provided the original work is properly cited, the use is non-commercial and no modifications or adaptations are made.

$\text{H}_2\text{S} < 11 \mu\text{M}$, non-quantitative Mo sequestration results in the enrichment of isotopically light Mo in sediments relative to the $\delta^{98}\text{Mo}$ composition of ambient water (e.g., Arnold et al., 2004; Bura-Nakić et al., 2018; Goldberg et al., 2012; Poulson et al., 2006; Scholz et al., 2017; Zheng et al., 2000). In contrast, under strongly sulfidic conditions exceeding the critical H_2S concentration, such as in some restricted marine basins, near-quantitative Mo sequestration can occur without any significant Mo isotope fractionation (e.g., Gordon et al., 2009; Helz et al., 2011; Neubert et al., 2008; Siebert et al., 2003).

Accurate interpretation of sedimentary Mo records requires a comprehensive understanding of its biogeochemical cycling, including Mo burial pathways and isotope fractionation process under anoxic conditions. Under sulfidic conditions, both iron sulfide minerals (pyrite) and organic matter play an important role in Mo sequestration and burial in marine sediments, serving as the main pathway for Mo burial (e.g., Ardakani et al., 2016, 2020; Chappaz et al., 2014; Dahl et al., 2016; Erickson & Helz, 2000; Helz & Vorliceck, 2019; Helz et al., 1996; Vorliceck et al., 2018; Wagner et al., 2017). Plentiful evidence exists for a strong correlation between organic matter and Mo abundances in modern and ancient sediments (e.g., Algeo & Lyons, 2006; Chappaz et al., 2014; Dahl et al., 2016; Dellwig et al., 2019; King et al., 2018; Piper & Perkins, 2004; Tribouvillard et al., 2004; Wagner et al., 2017). Recent studies have documented high Mo abundances in both live and dead cells of sulfate-reducing bacteria (Bao et al., 2018; Dahl et al., 2016), suggesting that preferential sequestration of Mo by organic matter might represent a main pathway for Mo burial on geological timescales, thereby explaining the observed close relationship between Mo and total organic carbon contents in ancient sediments (Dahl et al., 2016). Additionally, interactions between Mo and organic matter have been inferred from experimental studies showing that significant Mo isotope fractionation occurs during adsorption onto insolubilized humic acids, a surrogate for organic matter (from 0.82 to 1.79‰; King et al., 2018). However, little is known about the impact of microbial sulfate reduction on the degree of Mo isotope fractionation to date. Extensive microbial sulfate reduction is thought to have resulted in widespread euxinic conditions in ancient oceans (e.g., Arnold et al., 2004; Gill et al., 2011; Poulton et al., 2004), similar to the sulfidic conditions that typically prevail in sub-seafloor environments along modern ocean margins (e.g., Bowles et al., 2014; Jørgensen, 2021). In this regard, additional insight into how organic matter may affect Mo isotope fractionation would further advance our understanding of the linkages between organic matter, Mo, and sulfur cycling in both modern sulfidic pore-water environments and ancient euxinic oceans.

Involving sulfate-reducing bacteria, the anaerobic oxidation of methane and/or heavier hydrocarbon compounds at submarine seeps results in substantial alkalinity increase near the sediment-seawater interface, which typically leads to the precipitation of authigenic carbonate deposits (e.g., Boetius et al., 2000; Joye et al., 2004; Naehr et al., 2009; Peckmann & Thiel, 2004; Smrzka et al., 2019). Such seep carbonate rocks generally show moderate to significant Mo enrichments, which can reflect preferential sequestration of dissolved Mo under sulfidic conditions and/or the presence of early diagenetic sulfide minerals (e.g., Deng et al., 2020; Hu et al., 2014; Lin et al., 2021; Smrzka et al., 2020). For seep carbonate rocks dominated by aragonite, precipitation occurred near the sediment-seawater interface, hence recording information from both ambient bottom waters and sedimentary pore water (e.g., Hu et al., 2014; Lin et al., 2021). In marine sediments, Mo can be hosted in different phases, most notably in Fe-Mn oxide, organic matter, and iron sulfides (e.g., Dahl et al., 2016; Jia et al., 2023a; Nan et al., 2023; Phillips & Xu, 2021). Therefore, the $\delta^{98}\text{Mo}$ composition of bulk sediment or bulk authigenic carbonate samples integrates the sum of the $\delta^{98}\text{Mo}$ signature of each of these Mo-bearing phases. The use of $\delta^{98}\text{Mo}$ values of bulk-rock samples can consequently lead to inconsistent conclusions or even conclusions that contradict with other redox indicators such as iron speciation and redox sensitive element contents (Chen et al., 2021). To overcome this problem, the application of sequentially chemical extraction methods is particularly well suited to determine the elemental and isotopic characteristics of Mo hosted by different phases (Huang et al., 2023; Jia et al., 2023a). In authigenic carbonate rocks, sequential leaching can be used to selectively extract carbonate phases, which host Mo incorporated from ambient pore waters (Chen et al., 2021), but also the fraction of Mo bound to sulfides, which can form in the sediment by the combination of H_2S and sulfophilic elements (Hu et al., 2014; Smrzka et al., 2020). Additionally, sequential leaching can be used to extract the organic compounds preserved in authigenic carbonate rocks, which may contain critical information regarding the use of Mo by microorganisms that require Mo as a co-factor in enzymatic processes (Lee et al., 2022; Wang et al., 2019).

In a recent companion paper, we investigated the $\delta^{98}\text{Mo}$ composition of sequentially extracted carbonate and pyrite fractions from seep carbonate rocks, which provided new insights into the biogeochemical pathways of Mo during early diagenesis (Jia et al., 2023a). In the previous work focused more specifically on the “inorganic drivers” that control the degree of Mo isotope fractionation between seawater/pore-fluid and authigenic minerals.

However, despite evidence that the formation of authigenic carbonate and pyrite in reducing marine sediments is directly linked to methanotrophic and sulfate-reducing microorganisms, little is known about how Mo isotopes can be affected by microbial activity and how this may influence the burial pathway of Mo. These “organic drivers” are the subject of this study, where we focus on Mo abundances and isotopic ($\delta^{98}\text{Mo}$) compositions of both carbonate (*carb*) and organic (*OM*) fractions extracted from the same suite of seep carbonate rocks. The purpose is to improve our understanding of Mo isotope fractionation at submarine methane seeps and of the interaction of Mo with organic matter during microbial sulfate reduction. Such work is required to assess the potential use of Mo isotopes in sedimentary carbonate rocks as paleo-environmental proxy.

2. Samples and Analytical Methods

The seep carbonate rock samples used in this study are listed in Table 1. Authigenic carbonates from northern Gulf of Mexico seeps were collected at water depths varying between 260 and 700 m (Figure 1; Table 1; Roberts et al., 2010 and references therein), while those recovered at methane seeps from the South China Sea were recovered at 1,120 m water depth (Feng & Chen, 2015). More detailed information on studied seep carbonate rocks can be found elsewhere (Feng & Chen, 2015; Huang et al., 2020; Sun et al., 2020, 2021; Tong et al., 2019). The studied carbonate rocks result from sulfate-driven anaerobic oxidation of methane, a biogeochemical process involving microbial sulfate reduction. After collection and cleaning with deionized water, samples were ground using an agate mortar.

Bulk mineralogy and relative abundances of carbonate minerals were determined using a LabX X-ray diffraction-6100 diffractometer equipped with a diffracted beam graphite monochromator using $\text{CuK}\alpha$ radiation. The analytical conditions were set at 40 kV accelerating voltage and 30 mA current. The samples were scanned from 10° to 80° (2θ) at 0.02° per second with diverging, scattering, and receiving slits of 1° , 0.3° , and 1 mm, respectively. Quantification of MgCO_3 contents of carbonate minerals followed the procedures of Liang et al. (2017). Calcite with less than 5 mol% MgCO_3 , 5–20 mol% MgCO_3 , and 36–50 mol% MgCO_3 were defined as low-magnesium calcite (LMC), high-magnesium calcite (HMC), and dolomite, respectively (Burton, 1993; Burton & Walter, 1991).

To measure the carbon and sulfur contents, we first acidified the powdered samples with 4 M HCl for 12 hr to remove carbonate minerals. After acidification, the residue was centrifuged, thoroughly rinsed with deionized water, and freeze dried for carbon and sulfur analyses. The analyzed carbon in the residue represents total organic carbon (TOC). Since both volatile sulfide released during acidification and organic sulfur are negligible in the studied samples, the analyzed sulfur mainly corresponds to pyrite-bound sulfur (S_{py}). Carbon and sulfur were analyzed using a Vario EI-III Elemental Analyzer with an analytical precision of $<2\%$. For Samples GB260-1 and MC709-1 containing considerable amounts of barite (Huang et al., 2020; Sun et al., 2021), S_{py} contents were determined by a modified version of the chromium reduction method (Canfield et al., 1986; Hu et al., 2017). Samples were treated with 6 N HCl and 1 M CrCl_2 solutions in an O_2 -free reaction vessel with continuous N_2 flow, and the released H_2S gas was trapped in AgNO_3 solution and precipitated as Ag_2S . The contents of S_{py} were determined by weighting dried Ag_2S precipitates.

For stable carbon isotope ($\delta^{13}\text{C}$) and oxygen isotope ($\delta^{18}\text{O}$) analyses of the carbonate phases of seep carbonate rocks, the CO_2 fraction released after treatment of powdered samples with 100% phosphoric acid at 70°C was analyzed using a Gasbench II-Delta V Advantage mass spectrometer. For carbon stable isotope analysis of TOC of seep carbonate rocks, powdered samples were acidified following the above procedure, and the processed samples were combusted to CO_2 using an Elemental Analyzer (EA). The released CO_2 was subsequently analyzed using a Delta V Advantage mass spectrometer. Carbon and oxygen isotope values are expressed as δ notation relative to the Vienna-Pee Dee Belemnite (V-PDB) standard with precisions on the order of 0.1‰ (2SD) for both $\delta^{13}\text{C}$ and $\delta^{18}\text{O}$ values.

Following the analytical procedure of Hu et al. (2014), about 50 mg of powdered bulk-rock were digested using ultrapure concentrated HNO_3 and HF (185°C ; 36 hr) to determine trace element abundances of bulk rock. The resulting solution was evaporated to dryness and further digested in ultrapure HNO_3 (135°C ; 5 hr). For trace element analysis of the non-lithogenic fraction of seep carbonate rocks, about 50 mg of powdered samples were dissolved in a mixture of concentrated HNO_3 and HCl ($v/v = 3$) at 110°C for 24 hr. After centrifugation, the supernatant was evaporated to dryness, and the obtained residue was re-dissolved in 2% HNO_3 prior to analysis. Note that the non-lithogenic fraction mostly corresponds to the sum of carbonate, Fe-Mn oxide, sulfide, and

Table 1
Sample and Site Information of Seep Carbonate Rocks

Location	Site	Sample ID	Water depth (m)	References
Gulf of Mexico	GB260	GB260-1	460	Huang et al. (2020)
	GC140	GC140-1	260–510	Tong et al. (2019)
	GC232	GC232-1	570	Sun et al. (2020)
	MC709	MC709-1	680–700	Sun et al. (2021)
South China Sea	Site F	Site F-1	1,120	Feng and Chen (2015)
		Site F-2		

organic matter fractions associated with seep carbonate rocks, but can also contain a minor fraction of labile silicate minerals.

A sequential leaching procedure was conducted to determine the abundances of Mo and other trace elements in different phases of seep carbonate rocks, namely carbonate, Fe-Mn oxide, sulfide, and organic matter fractions. The carbonate-bound Mo was determined following leaching with 5% ultrapure acetic acid for 16 hr on ca. 300 mg of powdered samples (Rongemaille et al., 2011). While this leaching step also results in the removal of exchangeable Mo, this latter fraction remains small relative to the extracted Mo fraction derived from carbonate

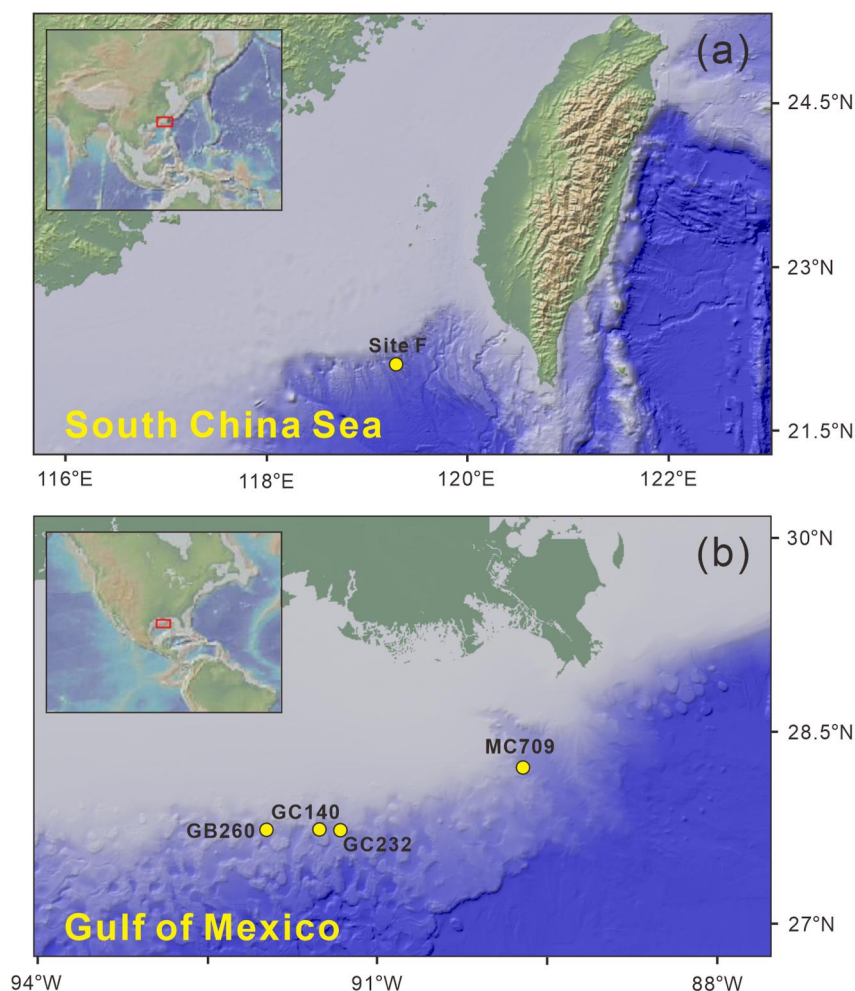


Figure 1. Maps showing the study areas and sampling sites. (a) Seep carbonate rocks were collected at Site F from the South China Sea. (b) Seep carbonate rocks were recovered at sites GC260, GC140, GC232, and MC709 from the Gulf of Mexico.

phases (Jia et al., 2023a). Next, Fe-Mn oxyhydroxide phases were extracted using a solution of 0.5 M hydroxylamine HCl adjusted to pH = 1.5 (16 hr) according to Tessier et al. (1979). Sulfide minerals, mainly pyrite, and associated Mo were subsequently dissolved by leaching with 3 M HNO₃ for 12 hr (Chao & Sanzolone, 1977). Note that at such molarity and at room temperature, the use of HNO₃ does not cause extensive oxidation of organic matter (Han et al., 2009). Finally, organic-bound Mo was extracted with 5% H₂O₂ (pH = 2) for 36 hr (Wang et al., 2019). All extractions were conducted on a mechanical shaker at room temperature. After each leaching step, the resulting residue obtained by centrifugation was thoroughly rinsed with deionized water (×4), and the combined supernatants were evaporated to dryness, and further digested in concentrated H₂O₂ and HNO₃. Prior to analysis, all the above processed leachates were re-dissolved in diluted 2% HNO₃. Trace element abundances in bulk-rock, non-lithogenic, carbonate, Fe-Mn oxide, sulfide, and organic matter fractions were determined using a Thermo Fisher iCAPRQ ICP-MS or a Thermo Fisher X series 2 ICP-MS. Certified reference materials (W-2a and BHVO-2) and a single standard solution of Mo were used for quality control with precision and accuracy both better than 5%.

All bulk-rock and non-lithogenic fractions as well as carbonate, pyrite, and organic matter phases of seep carbonate rocks extracted by sequential leaching were analyzed for Mo isotope compositions at the State Key Laboratory of Isotope Geochemistry, Guangzhou Institute of Geochemistry, Chinese Academy of Science using a Thermo-Fisher Scientific Neptune-Plus multi-collector inductively coupled plasma mass spectrometer. Note that the Mo fraction hosted in the Fe-Mn oxide phases extracted by sequential leaching was not analyzed for Mo isotopes due to methodological issues occurring during the corresponding chemical separation step by ion chromatography. Prior to chemical separation, a ¹⁰⁰Mo-⁹⁷Mo double spike was added to samples to correct instrumental mass bias and any other isotope fractionation during chemical preparation. Following the procedures of Li et al. (2014), chemical separation was performed by ion chromatography using N-benzoyl-N-phenyl hydroxylamine (BPHA) resin and a 6 M HF : 1 M HCl solution for Mo elution. Chemical yields of Mo after separation were usually higher than 90% with procedural blanks less than 0.23 ng of Mo, which corresponds to less than 1% of total Mo. Repeated measurements of a NIST SRM 3134 standard solution, USGS rock reference materials AGV-2, and IAPSO seawater standard produced δ⁹⁸Mo values of 0.25 ± 0.07‰ (2SD, n = 26), 0.08 ± 0.09‰ (2SD, n = 4), and 2.33 ± 0.02‰ (2SD, n = 4), respectively. These results are in agreement with reference values from the literature (Greber et al., 2012; Li et al., 2014; Zhao et al., 2016). The analytical error of δ⁹⁸Mo values was systematically <0.07‰ and typically less than 0.05‰ (2SD). The isotopic composition of Mo is expressed as δ⁹⁸Mo relative to the NIST SRM 3134 standard (δ⁹⁸Mo NIST3134 = +0.25‰), following Nägler et al. (2014):

$$\delta^{98}\text{Mo} (\text{‰}) = \left[\left(\frac{{}^{98}\text{Mo}/{}^{95}\text{Mo}}{\text{sample}} / \left(\frac{{}^{98}\text{Mo}/{}^{95}\text{Mo}}{\text{NIST3134}} - 1 \right) \right) \times 1000 + 0.25 \right] \quad (1)$$

3. Results

3.1. Carbonate Mineralogy, and δ¹³C and δ¹⁸O Compositions

The mineralogical compositions, as well as oxygen and carbon stable isotope compositions, of the samples analyzed are present in Table 2. Aragonite, LMC, HMC, and dolomite are the dominant minerals, with minor amounts of quartz, chlorite, and albite (Table 2). Total carbonate contents vary between 66 and 97 wt%. Pyrite was not detected by XRD analysis due to its low abundance. However, pyrite was widely observed using different types of microscopes (Feng & Chen, 2015; Huang et al., 2020; Jia et al., 2023a; Roberts et al., 2010).

The δ¹³C and δ¹⁸O values of the carbonate phase of the studied authigenic carbonate rocks (δ¹³C_{carb} and δ¹⁸O_{carb}) vary from −58.2‰ to −20.6‰ and from 2.8 to 4.6‰, respectively (Table 2). The δ¹³C values of organic matter (δ¹³C_{TOC}) are low, ranging from −46.7‰ to −23.4‰ (Table 2). The carbonate sample from site GB260 in the Gulf of Mexico is dominated by LMC with a δ¹³C_{carb} value of −49.8‰ and a δ¹³C_{TOC} value of −30.7‰. The sample recovered at site GC140 is rich in dolomite with a δ¹³C_{carb} value of −31.7‰ and a δ¹³C_{TOC} value of −23.4‰. The carbonate sample from site GC232 is dominated by aragonite, showing a δ¹³C_{carb} value of −20.6‰ and a δ¹³C_{TOC} value of −37.4‰. For sample at site MC709, the dominant carbonate mineral is LMC, yielding a δ¹³C_{carb} value of −27.4‰ and a δ¹³C_{TOC} value of −31.4‰. For Site F of the South China Sea, the carbonate samples are rich in HMC with δ¹³C_{carb} values from −58.2‰ to −47.4‰ and δ¹³C_{TOC} values from −46.7‰ to −42.7‰ (Table 2).

Table 2

Mineral, Carbon, and Oxygen Isotope Compositions of Seep Carbonate Rocks

Sample ID	Qz %	Ab %	Chl %	LMC %	Dol %	Arg %	HMC %	Carb. Cont. %	$\delta^{13}\text{C}_{\text{carb}} \text{‰}$	$\delta^{18}\text{O}_{\text{carb}} \text{‰}$	$\delta^{13}\text{C}_{\text{TOC}} \text{‰}$
GB260-1 ^a	2.8	0	0	97.2	0	0	0	97	-49.8	2.8	-30.7
GC140-1	5.7	4.5	0	0	76.0	0	13.7	90	-31.7	4.5	-23.4
GC232-1	5.4	0	0	3.8	0	90.8	0	95	-20.6	3.5	-37.4
MC709-1 ^a	4.6	0	0	95.4	0	0	0	95	-27.4	4.5	-31.4
Site F-1 ^a	16.2	6.2	7.7	0	0	18.1	51.9	70	-47.4	4.0	-42.7
Site F-2 ^a	17.1	9.6	7	0	0	0	66.3	66	-58.2	4.6	-46.7

Note. Qz, Ab, Chl, LMC, Dol, Arg, and HMC refer to quartz, albite, chlorite, low-magnesium calcite, dolomite, aragonite, and high-magnesium calcite, respectively. Carb. Cont.: Carbonate content. $\delta^{13}\text{C}_{\text{carb}}$ and $\delta^{18}\text{O}_{\text{carb}}$ represent $\delta^{13}\text{C}$ and $\delta^{18}\text{O}$ values of carbonate phase in the studied seep carbonates rocks, respectively. $\delta^{13}\text{C}_{\text{TOC}}$ indicates $\delta^{13}\text{C}$ values of total organic carbon in seep carbonate rocks. ^aData from Jia et al. (2023a).

3.2. Elemental Abundances

Except for the site GC232 sample, which displays a TOC content of 11.32% (Table 3) reflecting the influence of oil seepage (Sun et al., 2020), all other samples show a narrow range of TOC contents, falling between 0.53% and 2.10% (Table 2). The S_{py} content of the sample from site GB260 is low (0.03%), while other samples display higher S_{py} contents from 0.88% to 1.26% (Table 3). Non-lithogenic Mn ($\text{Mn}_{\text{non-litho}}$) and Fe ($\text{Fe}_{\text{non-litho}}$) contents range from 35 to 759 $\mu\text{g/g}$ and from 4,750 to 21,100 $\mu\text{g/g}$, respectively (Table 3). Non-lithogenic Mo ($\text{Mo}_{\text{non-litho}}$) contents vary from 3.5 to 12.9 $\mu\text{g/g}$, hence showing relative enrichment compared to the average Mo abundance in the Earth's upper continental crust (1.5 $\mu\text{g/g}$; McLennan, 2001; Table 3; Figure 2). The contents of $\text{Mo}_{\text{non-litho}}$ are in good agreement with the sum of all Mo fractions obtained by chemical extraction (ΣMo ; Figure 2), which confirms the reliability of our sequential leaching procedure. Relative to the total Mo budget of studied seep carbonate rocks (ΣMo), the proportion of pyrite-bound Mo (Mo_{py}) ranges from 52% to 86% (mean of $76 \pm 11\%$; 1SD; Figure 2). In comparison, the Mo fractions associated with extracted Fe-Mn oxide (Mo_{ox}) and organic matter (Mo_{OM}) phases account for <10% of the total Mo budget of studied carbonate rocks (Figure 2).

3.3. Molybdenum Isotope Compositions

In bulk-rock samples, $\delta^{98}\text{Mo}$ values vary between 1.02 and 2.07‰, averaging $1.61 \pm 0.36\text{‰}$ (1SD, $n = 6$; Figure 3). Similar to $\delta^{98}\text{Mo}_{\text{bulk}}$ values, $\delta^{98}\text{Mo}$ values of the non-lithogenic fraction ($\delta^{98}\text{Mo}_{\text{non-litho}}$) range from 1.09 to 2.12‰ with an average of $1.62 \pm 0.36\text{‰}$ (1SD, $n = 6$; Figure 3). Generally, the $\delta^{98}\text{Mo}$ composition of the pyrite fraction of seep carbonate rocks ($\delta^{98}\text{Mo}_{\text{py}}$), varying from 1.07 to 2.10‰ with an average of $1.65 \pm 0.40\text{‰}$ (1SD, $n = 6$), is close to the corresponding $\delta^{98}\text{Mo}_{\text{bulk}}$ and $\delta^{98}\text{Mo}_{\text{non-litho}}$ values (Figure 3). This indicates that $\delta^{98}\text{Mo}_{\text{py}}$ largely controls the $\delta^{98}\text{Mo}_{\text{non-litho}}$ signature of studied seep carbonate rocks (Figure 2). The Mo isotope values of the carbonate fraction of seep carbonate rocks ($\delta^{98}\text{Mo}_{\text{carb}}$) are the highest among all

Table 3

Contents of Total Organic Carbon (TOC), Pyrite Sulfur (S_{py}), Manganese (Mn), and Iron (Fe) of Seep Carbonates and Molybdenum (Mo) of Different Phases of Seep Carbonate Rocks

Sample ID	TOC %	S_{py} %	$\text{Mo}_{\text{non-litho}}$ $\mu\text{g/g}$	Mo_{carb} $\mu\text{g/g}$	Mo_{ox} $\mu\text{g/g}$	Mo_{py} $\mu\text{g/g}$	Mo_{OM} $\mu\text{g/g}$	$\text{Mn}_{\text{non-litho}}$ $\mu\text{g/g}$	$\text{Fe}_{\text{non-litho}}$ $\mu\text{g/g}$
GB260-1 ^a	1.88	0.03	3.5	0.22	0.12	3.16	0.34	231	8,410
GC140-1	0.53	1.26	6.0	0.83	0.32	4.58	0.48	128	9,370
GC232-1	11.3	1.13	8.3	1.51	0.35	5.71	0.11	35	4,750
MC709-1 ^a	2.10	0.88	5.8	0.29	0.33	5.84	0.39	759	11,300
Site F-1 ^a	0.58	0.99	12.9	0.47	0.78	9.77	0.33	225	21,100
Site F-2 ^a	0.69	1.22	12.5	4.26	1.23	7.00	0.86	303	18,700

Note. $\text{Mo}_{\text{non-litho}}$, Mo_{carb} , Mo_{ox} , Mo_{py} , and Mo_{OM} refer to Mo contents of non-lithogenic, carbonate, Fe-Mn oxide, pyrite, and organic matter fractions of seep carbonate rocks, respectively. $\text{Mn}_{\text{non-litho}}$ and $\text{Fe}_{\text{non-litho}}$ indicate Mn and Fe contents of non-lithogenic fractions of seep carbonate rocks, respectively. ^aData from Jia et al. (2023a).

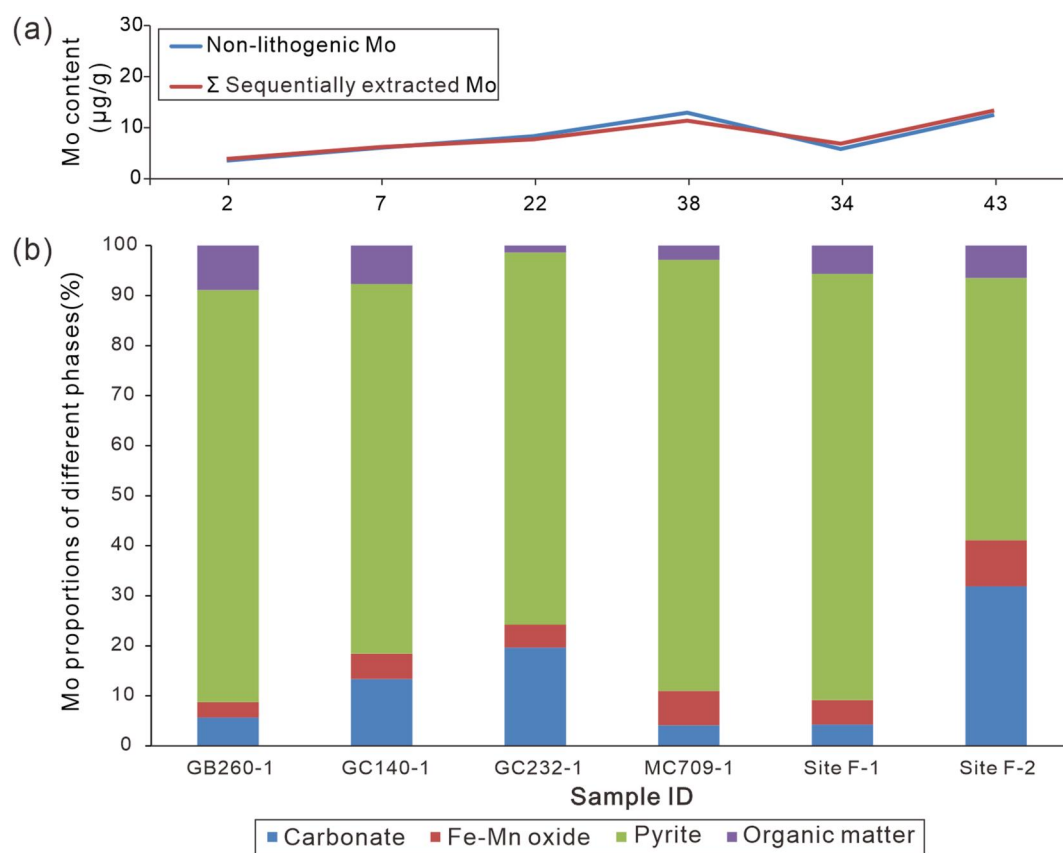


Figure 2. Molybdenum (Mo) contents and proportions of different phases for seep carbonate rocks. The upper graph shows the non-lithogenic Mo contents and the sum of Mo contents hosted in different phases by sequential chemical extraction. The lower graph presents Mo relative proportions of different phases (i.e., carbonate, Fe-Mn oxide, pyrite, and organic matter). Data for samples GB260-1, MC709-1, Site F-1, and Site F-2 are from Jia et al. (2023a).

studied fractions, varying from 1.54 to 2.64‰ with an average of $2.07 \pm 0.39\text{‰}$ (1SD, $n = 6$; Figure 3). In contrast, $\delta^{98}\text{Mo}$ values of the organic fraction of seep carbonate rocks ($\delta^{98}\text{Mo}_{\text{OM}}$) are the lowest among all studied fractions, ranging from 0.77 to 1.80‰ with an average of $1.24 \pm 0.36\text{‰}$ (1SD, $n = 6$; Figure 3). Therefore, $\delta^{98}\text{Mo}_{\text{py}}$ values are generally lower than the corresponding $\delta^{98}\text{Mo}_{\text{carb}}$ values but higher than the corresponding $\delta^{98}\text{Mo}_{\text{OM}}$ values (Figure 3).

4. Discussion

4.1. Biogeochemical Processes and Conditions During Seep Carbonate Formation

Sulfate-driven anaerobic oxidation of methane (AOM) at seeps results in the release of large amounts of ^{13}C -depleted bicarbonate. This process increases pore-water alkalinity and leads to the formation of ^{13}C -depleted authigenic carbonates (e.g., Boetius et al., 2000; Peckmann & Thiel, 2004). As a result, carbonate rocks found in seep environments commonly exhibit highly negative $\delta^{13}\text{C}_{\text{carb}}$ values, commonly lower than $\delta^{13}\text{C}$ values of marine organic matter. Such negative $\delta^{13}\text{C}$ values typically serve as diagnostic features for the occurrence of AOM in the marine environment (e.g., Peckmann & Thiel, 2004). The $\delta^{13}\text{C}_{\text{carb}}$ values lower than -47‰ obtained for samples of site GB260 from the Gulf of Mexico and Site F from the South China Sea indicate that carbonate formation was driven by AOM, inheriting the carbon isotope composition of the methane-rich fluid sources (Table 2; Feng & Chen, 2015; Huang et al., 2020). The occurrence of dolomite typified by a $\delta^{13}\text{C}_{\text{carb}}$ value of -31.7‰ for the sample from site GC140 (Table 2) is consistent with previous results (Tong et al., 2019). Based on the evidence for steep $\delta^{18}\text{O}/\delta^{34}\text{S}$ slopes for carbonate-associated sulfate and high $\delta^{34}\text{S}$ values of sulfide minerals (Tong et al., 2019), the GC140 carbonates most likely formed in a relatively low sulfate, high-sulfide environment that was generated by prolonged sulfate reduction.

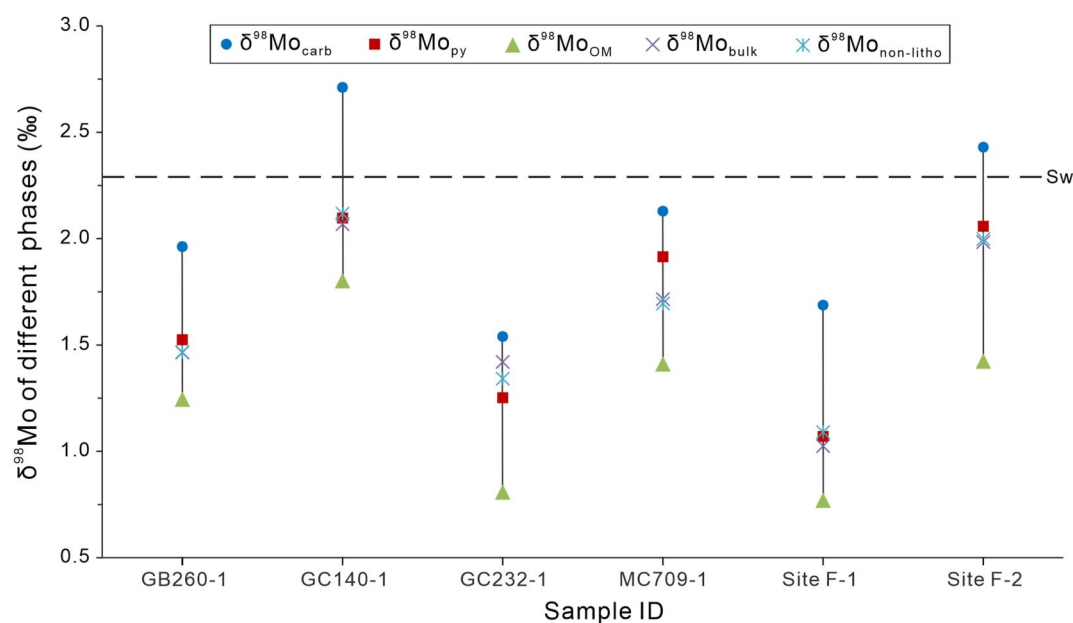


Figure 3. $\delta^{98}\text{Mo}$ values of different phases of seep carbonate rocks, including carbonate ($\delta^{98}\text{Mo}_{\text{carb}}$), pyrite ($\delta^{98}\text{Mo}_{\text{py}}$), organic matter ($\delta^{98}\text{Mo}_{\text{OM}}$), bulk-rock ($\delta^{98}\text{Mo}_{\text{bulk}}$), and non-lithogenic phases ($\delta^{98}\text{Mo}_{\text{non-litho}}$). The dashed line marks the modern seawater $\delta^{98}\text{Mo}$ value. Values for $\delta^{98}\text{Mo}_{\text{carb}}$, $\delta^{98}\text{Mo}_{\text{py}}$, $\delta^{98}\text{Mo}_{\text{bulk}}$, and $\delta^{98}\text{Mo}_{\text{non-litho}}$ in GB260-1, MC709-1, Site F-1, and Site F-2 samples are from Jia et al. (2023a).

Concerning seep carbonate rocks from sites GC232 and MC709, the obtained data for TOC and total nitrogen contents, $\delta^{13}\text{C}_{\text{TOC}}$ values, and $\delta^{34}\text{S}$ values of sulfides and organic sulfur point toward environmental conditions associated with the biodegradation of heavy hydrocarbons and other oil derived compounds by sulfate-reducing bacteria (cf. Joye et al., 2004; Naehr et al., 2009; Sun et al., 2020). This conclusion is supported by high contents Mo_{py} and S_{py} (Table 3). For surface sediments not affected by seepage from the South China Sea and the Gulf of Mexico, $\delta^{13}\text{C}_{\text{TOC}}$ values are -20‰ and -22‰ , respectively (Chen et al., 2012; Eadie et al., 1978; LaRowe et al., 2020). In contrast, for all the seep carbonate rocks investigated in this study, $\delta^{13}\text{C}_{\text{TOC}}$ values lower than -22‰ indicate a contribution of dissolved inorganic carbon resulting from the oxidation of methane and oil components, with sulfate as the major electron acceptor (Table 2; Feng et al., 2021). Highly ^{13}C -depleted TOC with $\delta^{13}\text{C}$ values as low as -46.7‰ for Site F (Table 2) reflects the local abundance of methanotrophic biomass and pronounced AOM (cf. Feng et al., 2021; Wegener et al., 2008). In summary, the formation processes and conditions of the studied seep carbonate rocks reflect the consumption of methane and the degradation of oil, both driven by microbial sulfate reduction.

4.2. $\delta^{98}\text{Mo}$ Patterns of Different Phases of Seep Carbonate Rocks

The circumstance that $\text{Mo}_{\text{non-litho}}$ contents generally agree with the sum of all Mo fractions obtained by chemical extraction in this study provides reassuring evidence for the reliability of our sequential leaching procedure (Figure 2a). Likewise, such evidence for near-quantitative extraction of Mo during the sequential leaching procedure also suggests that any experimental Mo isotope fractionation induced by leaching should be negligible. This interpretation agrees with the observation that pyrite dominates (a) the Mo budget as well as (b) the $\delta^{98}\text{Mo}$ signature of seep carbonate rocks (Figures 2 and 3). As mentioned above, at the critical threshold H_2S concentrations of 11–100 μM , a $\delta^{98}\text{Mo}$ offset of ca. 0.5–0.7‰ exists between sequestered Mo and seawater/pore water Mo (e.g., Bura-Nakić et al., 2018; Bura-Nakić et al., 2020; Gordon et al., 2009; He et al., 2021; Hutchings et al., 2020; Nägler et al., 2011; Neubert et al., 2008; Poulson et al., 2006; Romaniello et al., 2016). Offsets smaller than 0.7‰ between $\delta^{98}\text{Mo}_{\text{py}}$ and ambient water $\delta^{98}\text{Mo}$ therefore probably result from Mo isotope fractionation at or above the near-critical H_2S concentration (Figure 3; Lin et al., 2021). In contrast, the observation of isotopic offsets larger than 0.7‰ between $\delta^{98}\text{Mo}_{\text{py}}$ and ambient water $\delta^{98}\text{Mo}$ instead suggests an additional contribution of isotopically light Mo to Mo_{py} (Figure 3). It has been shown that isotopically light Mo is preferentially adsorbed

onto Fe-Mn oxides (e.g., Barling & Anbar, 2004; Chen et al., 2022; Eroglu et al., 2020; Goldberg et al., 2009; Scholz et al., 2017; Siebert et al., 2003; Wasylenki et al., 2008). In the studied seep carbonate rocks, the Mo fractions associated with extracted organic matter are also generally typified by the enrichment of isotopically light Mo, with $\delta^{98}\text{Mo}_{\text{OM}}$ lower than $\delta^{98}\text{Mo}_{\text{py}}$ values (Figure 3). Accordingly, the relatively light $\delta^{98}\text{Mo}_{\text{py}}$ compositions associated with pyrite—a mineral typically composed of crystal aggregates progressively forming during early diagenetic processes (Berner, 1970, 1984; Domingos et al., 2023)—are expected to be inherited from the release of isotopically light Mo during the course of early diagenesis, following both Fe-Mn oxide reduction and organic matter as well as oil remineralization by sulfate reduction.

Recent work has shown that $\delta^{98}\text{Mo}_{\text{carb}}$ values faithfully reflect the $\delta^{98}\text{Mo}$ composition of pore waters since only negligible Mo isotope fractionation is thought to occur during calcite precipitation (Chen et al., 2021). The degree of Mo isotope fractionation during the adsorption of pore water Mo onto organic matter can thus be estimated by the difference between $\delta^{98}\text{Mo}_{\text{carb}}$ and $\delta^{98}\text{Mo}_{\text{OM}}$ ($\Delta^{98}\text{Mo}_{\text{carb-OM}}$). In this study, the obtained $\Delta^{98}\text{Mo}_{\text{carb-OM}}$ values vary from 0.72 to 1.01‰, that is, a range that is similar to that previously observed between dissolved Mo and insoluble humic acids (King et al., 2018). To the best of our knowledge, this finding represents the first report of the extent of Mo isotope fractionation during adsorption of Mo onto organic matter in the marine environment, being fully consistent with previous inferences derived from experimental work (Biswas et al., 2009; King et al., 2018).

4.3. Mo Isotope Fractionation During Sulfate Reduction

Despite the evidence for a close interaction between Mo and both live and dead cells of sulfate-reducing bacteria (Bao et al., 2018; Dahl et al., 2016), little is known about the degree of Mo isotope fractionation during Mo sequestration by organic matter. Marine seeps—with their locally enhanced sulfate reduction and a high abundance of sulfate-reducing bacteria—are typified by (a) prominent pyrite production, (b) high abundance of authigenic Mo in the sediments, and (c) the occurrence of highly depleted $\delta^{13}\text{C}$ signatures in both organic matter and authigenic carbonate rocks (e.g., Feng et al., 2021; Hu et al., 2014; Peckmann & Thiel, 2004). Methanotrophic archaea and associated sulfate-reducing bacteria assimilate highly ^{13}C -depleted bicarbonate and methane into their biomass (e.g., Bowles et al., 2020; Osorio-Rodriguez et al., 2023; Wegener et al., 2008), contributing to the highly ^{13}C -depleted TOC at seeps (e.g., Feng et al., 2021). Enhanced sulfate reduction at seeps can be generally inferred from more negative $\delta^{13}\text{C}_{\text{carb}}$ and $\delta^{13}\text{C}_{\text{TOC}}$ values, although the fact that methane-rich fluids at seeps worldwide carry distinctive and variable $\delta^{13}\text{C}$ compositions (due to different origins, such as thermogenic and biogenic methane) complicates the use of $\delta^{13}\text{C}_{\text{carb}}$ and $\delta^{13}\text{C}_{\text{TOC}}$ as a proxy for the intensity of sulfate reduction. Pyrite and Mo contents in authigenic carbonates can provide independent constraints on the degree of sulfate reduction (e.g., Gong et al., 2018) as they result from enhanced sulfate reduction and the consequent H_2S production.

In this study, we found that certain distinctive diagnostic features (S_{py} , Mo_{py} , $\delta^{13}\text{C}_{\text{carb}}$, and $\delta^{13}\text{C}_{\text{TOC}}$) associated with enhanced sulfate reduction are consistently linked to higher $\Delta^{98}\text{Mo}_{\text{carb-OM}}$ values (Figure 4; Table 3). For instance, for Site F of the South China Sea, a higher $\Delta^{98}\text{Mo}_{\text{carb-OM}}$ value along with higher S_{py} and Mo_{py} contents suggests enhanced sulfate reduction and corresponding sulfate-reducing bacterial activity. In seepage areas, any increase in the rate of sulfate reduction is accompanied by enhanced metabolic activity and/or an increase in the biomass of sulfate-reducing bacteria (Glass et al., 2014; Osorio-Rodriguez et al., 2023). Such enhanced microbial activity is likely to come along with a greater sequestration of light Mo isotopes from the surrounding pore water onto the microbially derived organic matter, hence resulting in enhanced Mo isotope fractionation and higher $\Delta^{98}\text{Mo}_{\text{carb-OM}}$ values (Figure 4). Therefore, our data suggest that the difference in $\delta^{98}\text{Mo}$ composition between the carbonate fractions and the organic matter fractions preserved in the authigenic carbonates can provide insights into the effect of organic matter on dissolved Mo during sulfate reduction. On this basis, we suggest that $\Delta^{98}\text{Mo}_{\text{carb-OM}}$ derived from authigenic carbonate rocks can be used to assess the extent of bacterial sulfate reduction, with higher $\Delta^{98}\text{Mo}_{\text{carb-OM}}$ values indicating enhanced sulfate reduction. Euxinic conditions (i.e., low-oxygen and high-sulfide levels in the water column) were prevalent in ancient oceans (e.g., Gill et al., 2011; Poulton et al., 2004), where sulfate-reducing bacteria likely played a significant role in Mo burial (Dahl et al., 2016). Regardless of their origin—carbonate precipitation related to sulfate reduction in the water column or AOM in the sediment—the interaction between organic matter and dissolved Mo during sulfate reduction

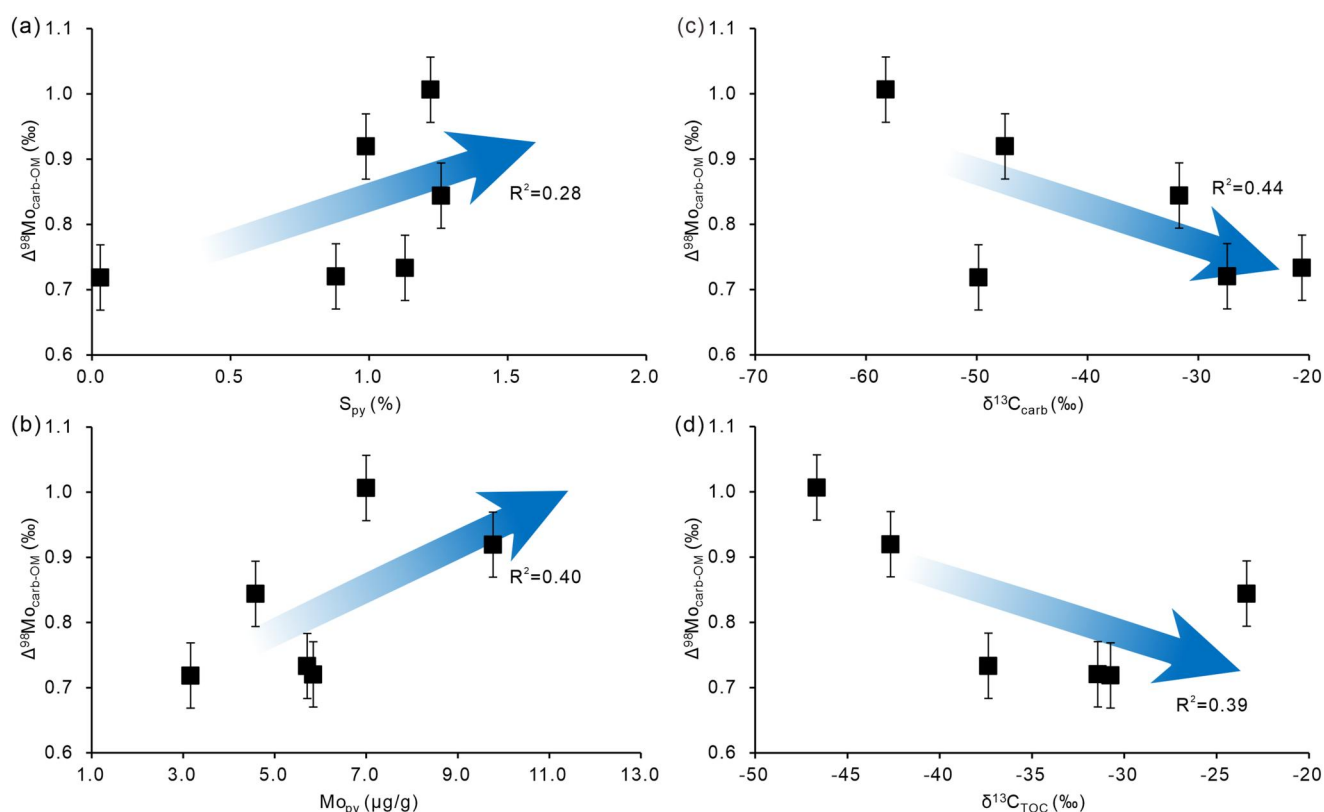


Figure 4. Difference of $\delta^{98}\text{Mo}$ values between carbonate and organic matter phases in seep carbonate rocks ($\Delta^{98}\text{Mo}_{\text{carb-OM}}$) versus (a) contents of pyrite sulfur (S_{py}), (b) contents of pyrite bound Mo (Mo_{py}), (c) $\delta^{13}\text{C}$ values of carbonate ($\delta^{13}\text{C}_{\text{carb}}$), and (d) $\delta^{13}\text{C}$ values of total organic carbon ($\delta^{13}\text{C}_{\text{TOC}}$) in seep carbonate rocks. S_{py} , Mo_{py} , $\delta^{13}\text{C}_{\text{carb}}$, $\delta^{98}\text{Mo}_{\text{carb}}$ and $\delta^{13}\text{C}_{\text{TOC}}$ data for samples GB260-1, MC709-1, Site F-1, and Site F-2 are from Jia et al. (2023a).

should be preserved in all types of marine carbonate rocks. Therefore, the potential $\Delta^{98}\text{Mo}_{\text{carb-OM}}$ proxy of sedimentary carbonate rocks holds promise as a tool for tracing the intensity of bacterial sulfate reduction and the cycling of Mo and sulfur in ancient marine sediments.

5. Conclusions and Perspectives

Fractions of molybdenum (Mo) bound to carbonate, pyrite, and organic phases of seep carbonate rocks from four sites of the Gulf of Mexico and one site from the South China Sea were isolated using a sequential leaching procedure and analyzed for Mo contents and isotopic compositions. Our data indicate that pyrite dominates the Mo budget and the $\delta^{98}\text{Mo}$ composition of seep carbonate rocks. The observed $\delta^{98}\text{Mo}$ values in leached fractions are largely explained by the fact that Mo isotopes fractionate upon sequestration under sulfidic conditions and that early diagenetic remobilization of both Fe-Mn oxides and organic matter release an isotopically light fraction of Mo, which can be subsequently incorporated into authigenic pyrite. A striking result of our study is the observation that the degree of Mo isotope decoupling between the leached carbonate ($\delta^{98}\text{Mo}_{\text{carb}}$) and organic ($\delta^{98}\text{Mo}_{\text{OM}}$) fractions exhibits an apparent correlation with geochemical markers of the intensity of microbial sulfate reduction. Higher $\Delta^{98}\text{Mo}_{\text{carb-OM}}$ values at sites typified by greater sulfate reduction rates suggest that sulfate-reducing bacteria preferentially absorb isotopically light Mo, causing larger Mo isotope fractionation ($\sim 1\text{‰}$). The suggested linkage between the degree of Mo isotope fractionation and the intensity of sulfate reduction should be investigated further in future experimental work. Considering that euxinic conditions were once widespread in ancient oceans at times where sulfidic conditions probably favored Mo burial, the new $\Delta^{98}\text{Mo}_{\text{carb-OM}}$ proxy should be applied in future studies on ancient carbonate rocks to reconstruct the intensity of bacterial sulfate reduction in marine sediments, serving as an independent proxy for tracing sulfur cycling and Mo burial.

Data Availability Statement

All the data used in the study are publicly available in the Mendeley Data Repository (Jia et al., 2023b).

Acknowledgments

Carbonate samples from the Gulf of Mexico were collected during projects funded by the Bureau of Ocean Energy Management and NOAA's National Undersea Research Program. We thank the crew of R/V *Xiangyanghong-09* as well as the operation teams of *Jiaolong* for their professional support during cruises in the South China Sea. This work was partially supported by the National Natural Science Foundation of China (42225603 and 42176056) and the Shanghai Pujiang Program (Grant 21PJ1404700). Insightful comments from the editor Dr. Branwen Williams and two anonymous reviewers helped to improve the manuscript.

References

- Algeo, T. J., & Lyons, T. W. (2006). Mo-total organic carbon covariation in modern anoxic marine environments: Implications for analysis of paleoredox and paleohydrographic conditions. *Paleoceanography and Paleoclimatology*, 21(1), PA1016. <https://doi.org/10.1029/2004PA001112>
- Ardakani, O. H., Chappaz, A., Sanei, H., & Mayer, B. (2016). Effect of thermal maturity on remobilization of molybdenum in black shales. *Earth and Planetary Science Letters*, 449, 311–320. <https://doi.org/10.1016/j.epsl.2016.06.004>
- Ardakani, O. H., Hlohowskyj, S. R., Chappaz, A., Sanei, H., Liseroudi, M. H., & Wood, J. M. (2020). Molybdenum speciation tracking hydrocarbon migration in fine-grained sedimentary rocks. *Geochimica et Cosmochimica Acta*, 283, 136–148. <https://doi.org/10.1016/j.gca.2020.06.006>
- Arnold, G. L., Anbar, A. D., Barling, J., & Lyons, T. W. (2004). Molybdenum isotope evidence for widespread anoxia in mid-Proterozoic oceans. *Science*, 304(5667), 87–90. <https://doi.org/10.1126/science.1091785>
- Bao, P., Li, G., Sun, G., Xu, Y., Meharg, A. A., & Zhu, Y. (2018). The role of sulfate reducing prokaryotes in the coupling of element biogeochemical cycling. *Science of the Total Environment*, 613–614, 398–408. <https://doi.org/10.1016/j.scitotenv.2017.09.062>
- Barling, J., & Anbar, A. D. (2004). Molybdenum isotope fractionation during adsorption by manganese oxides. *Earth and Planetary Science Letters*, 217(3–4), 315–329. [https://doi.org/10.1016/S0012-821X\(03\)00608-3](https://doi.org/10.1016/S0012-821X(03)00608-3)
- Barling, J., Arnold, G. L., & Anbar, A. D. (2001). Natural mass dependent variations in the isotopic composition of molybdenum. *Earth and Planetary Science Letters*, 193(3–4), 447–457. [https://doi.org/10.1016/S0012-821X\(01\)00514-3](https://doi.org/10.1016/S0012-821X(01)00514-3)
- Berner, R. A. (1970). Sedimentary pyrite formation. *American Journal of Science*, 268, 1–23. <https://doi.org/10.2475/ajs.268.1.1>
- Berner, R. A. (1984). Sedimentary pyrite formation: An update. *Geochimica et Cosmochimica Acta*, 48(4), 605–615. [https://doi.org/10.1016/0016-7037\(84\)90089-9](https://doi.org/10.1016/0016-7037(84)90089-9)
- Biswas, K., Woodards, N. A., Xu, H., & Barton, L. L. (2009). Reduction of molybdate by sulfate-reducing bacteria. *Biomaterials*, 22(1), 131–139. <https://doi.org/10.1007/s10534-008-9198-8>
- Boetius, A., Ravensschlag, K., Schubert, C. J., Rickert, D., Widdel, F., Gieseke, A., et al. (2000). A marine microbial consortium apparently mediating anaerobic oxidation of methane. *Nature*, 407(6804), 623–626. <https://doi.org/10.1038/35036572>
- Bowles, M. W., Mogollón, J. M., Kasten, S., Zabel, M., & Hinrichs, K.-U. (2014). Global rates of marine sulfate reduction and implications for sub-sea-floor metabolic activities. *Science*, 344(6186), 889–891. <https://doi.org/10.1126/science.1249213>
- Bowles, M. W., Samarkin, V. A., Hunter, K. S., Finke, N., Teske, A. P., Gircuis, P. R., & Joye, S. B. (2020). Remarkable capacity for anaerobic oxidation of methane at high methane concentration. *Geophysical Research Letters*, 46(21), 12192–12201. <https://doi.org/10.1029/2019GL084375>
- Bura-Nakić, E., Andersen, M. B., Archer, C., De Souza, G. F., Margaš, M., & Vance, D. (2018). Coupled Mo-U abundances and isotopes in a small marine euxinic basin: Constraints on processes in euxinic basins. *Geochimica et Cosmochimica Acta*, 222, 212–229. <https://doi.org/10.1016/j.gca.2017.10.023>
- Bura-Nakić, E., Sondi, I., Mikac, N., & Andersen, M. B. (2020). Investigating the molybdenum and uranium redox proxies in a modern shallow anoxic carbonate rich marine sediment setting of the Malo Jezero (Mljet Lakes, Adriatic Sea). *Chemical Geology*, 533, 119441. <https://doi.org/10.1016/j.chemgeo.2019.119441>
- Burton, E. A. (1993). Controls on marine carbonate cement mineralogy: Review and reassessment. *Chemical Geology*, 105(1–3), 163–179. [https://doi.org/10.1016/0009-2541\(93\)90124-2](https://doi.org/10.1016/0009-2541(93)90124-2)
- Burton, E. A., & Walter, L. M. (1991). The effects of PCO₂ and temperature on magnesium incorporation in calcite in seawater and MgCl₂-CaCl₂ solutions. *Geochimica et Cosmochimica Acta*, 55(3), 777–785. [https://doi.org/10.1016/0016-7037\(91\)90341-2](https://doi.org/10.1016/0016-7037(91)90341-2)
- Canfield, D. E., Raiswell, R., Westrich, J. T., Reaves, C. M., & Berner, R. A. (1986). The use of chromium reduction in the analysis of reduced inorganic sulfur in sediments and shales. *Chemical Geology*, 54(1–2), 149–155. [https://doi.org/10.1016/0009-2541\(86\)90078-1](https://doi.org/10.1016/0009-2541(86)90078-1)
- Chao, T., & Sanzalone, R. F. (1977). Chemical dissolution of sulfide minerals. *Journal of Research of the U. S. Geological Survey*, 5, 409–412.
- Chappaz, A., Lyons, T. W., Gregory, D. D., Reinhard, B. C., Gill, C., & Large, R. R. (2014). Does pyrite act as an important host for molybdenum in modern and ancient euxinic sediments? *Geochimica et Cosmochimica Acta*, 126, 112–122. <https://doi.org/10.1016/j.gca.2013.10.028>
- Chen, F., Chen, J., Jin, H., & Li, H. (2012). Correlation of δ¹³C_{org} in surface sediments with sinking particulate matter in South China Sea and implication for reconstructing paleo-environment. *Acta Sedimentologica Sinica*, 30, 340–345. (in Chinese with English abstract).
- Chen, S., Peng, X., Li, J., Lin, Z., Li, H., Wei, G., et al. (2022). Extremely light molybdenum isotope signature of sediments in the Mariana Trench. *Chemical Geology*, 605, 120959. <https://doi.org/10.1016/j.chemgeo.2022.120959>
- Chen, X., Ling, H. F., Vance, D., Shields-Zhou, G. A., Zhu, M., Poulton, S. W., et al. (2015). Rise to modern levels of ocean oxygenation coincided with the Cambrian radiation of animals. *Nature Communications*, 6(1), 7142. <https://doi.org/10.1038/ncomms8142>
- Chen, X., Romaniello, S. J., & Anbar, A. D. (2021). Preliminary exploration of molybdenum isotope fractionation during coprecipitation of molybdate with abiotic and microbial calcite. *Chemical Geology*, 566, 120102. <https://doi.org/10.1016/j.chemgeo.2021.120102>
- Cheng, M., Li, C., Jin, C., Wang, H., Algeo, T. J., Lyons, T. W., et al. (2020). Evidence for high organic carbon export to the early Cambrian seafloor. *Geochimica et Cosmochimica Acta*, 287, 125–140. <https://doi.org/10.1016/j.gca.2020.01.050>
- Colodner, D., Edmond, J., & Boyle, E. (1995). Rhenium in the Black Sea: Comparison with molybdenum and uranium. *Earth and Planetary Science Letters*, 131(1–2), 1–15. [https://doi.org/10.1016/0012-821X\(95\)00010-A](https://doi.org/10.1016/0012-821X(95)00010-A)
- Dahl, T. W., Chappaz, A., Hoek, J., McKenzie, C. J., Svane, S., & Canfield, D. E. (2016). Evidence of molybdenum association with particulate organic matter under sulfidic conditions. *Geobiology*, 15(2), 311–323. <https://doi.org/10.1111/gbi.12220>
- Dellwig, O., Wegwerth, A., Schnetger, B., Schulz, H., & Arz, H. W. (2019). Dissimilar behaviors of the geochemical twins W and Mo in hypoxic-euxinic marine basins. *Earth-Science Reviews*, 193, 1–23. <https://doi.org/10.1016/j.earscirev.2019.03.017>
- Deng, Y., Chen, F., Hu, Y., Guo, Q., Cao, J., Chen, H., et al. (2020). Methane seepage patterns during the middle Pleistocene inferred from molybdenum enrichments of seep carbonates in the South China Sea. *Ore Geology Reviews*, 125, 103701. <https://doi.org/10.1016/j.oregeorev.2020.103701>
- Dickson, A. J. (2017). A molybdenum-isotope perspective on Phanerozoic deoxygenation events. *Nature Geoscience*, 10, 721–726. <https://doi.org/10.1038/NNGEO3028>

- Dickson, A. J., Cohen, A. S., & Coe, A. L. (2014). Continental margin molybdenum isotope signatures from the early Eocene. *Earth and Planetary Science Letters*, *404*, 389–395. <https://doi.org/10.1016/j.epsl.2014.08.004>
- Domingos, J. M., Runge, E., Dreher, C., Chiu, T. H., Shuster, J., Fischer, S., et al. (2023). Inferred pyrite growth via the particle attachment pathway in the presence of trace metals. *Geochemical Perspectives Letters*, *26*, 14–19. <https://doi.org/10.7185/geochemlet.2318>
- Eadie, B. J., Jeffrey, L. M., & Sackett, W. M. (1978). Some observations on the stable carbon isotope composition of dissolved and particulate organic carbon in the marine environment. *Geochimica et Cosmochimica Acta*, *42*(8), 1265–1269. [https://doi.org/10.1016/0016-7037\(78\)90120-5](https://doi.org/10.1016/0016-7037(78)90120-5)
- Emerson, S. R., & Huested, S. S. (1991). Ocean anoxia and the concentrations of molybdenum and vanadium in seawater. *Marine Chemistry*, *34*(3–4), 177–196. [https://doi.org/10.1016/0304-4203\(91\)90002-E](https://doi.org/10.1016/0304-4203(91)90002-E)
- Erickson, B. E., & Helz, G. R. (2000). Molybdenum (VI) speciation in sulfidic waters: Stability and lability of thiomolybdates. *Geochimica et Cosmochimica Acta*, *64*(7), 1149–1158. [https://doi.org/10.1016/S0016-7037\(99\)00423-8](https://doi.org/10.1016/S0016-7037(99)00423-8)
- Eroglu, S., Scholz, F., Frank, M., & Siebert, C. (2020). Influence of particulate versus diffusive molybdenum supply mechanisms on the molybdenum isotope composition of continental margin sediments. *Geochimica et Cosmochimica Acta*, *273*, 51–69. <https://doi.org/10.1016/j.gca.2020.01.009>
- Feng, D., & Chen, D. (2015). Authigenic carbonates from an active cold seep of the northern South China Sea: New insights into fluid sources and past seepage activity. *Deep-Sea Research II*, *122*, 74–83. <https://doi.org/10.1016/j.dsr2.2015.02.003>
- Feng, D., Pohlman, J. W., Peckmann, J., Sun, Y., Hu, Y., Roberts, H. H., & Chen, D. (2021). Contribution of deep-sourced carbon from hydrocarbon seeps to sedimentary organic carbon: Evidence from radiocarbon and stable isotope geochemistry. *Chemical Geology*, *585*, 120572. <https://doi.org/10.1016/j.chemgeo.2021.120572>
- Gill, B. C., Lyons, T. W., Young, S. A., Kump, L. R., Knoll, A. H., & Saltzman, M. R. (2011). Geochemical evidence for widespread euxinia in the Later Cambrian Ocean. *Nature*, *469*(7328), 80–83. <https://doi.org/10.1038/nature09700>
- Glass, J. B., Yu, H., Steele, J. A., Dawson, K. S., Sun, S., Chourey, K., et al. (2014). Geochemical, metagenomic and metaproteomic insights into trace metal utilization by methane-oxidizing microbial consortia in sulphidic marine sediments. *Environmental Microbiology*, *16*(6), 1592–1611. <https://doi.org/10.1111/1462-2920.12314>
- Goldberg, T., Archer, C., Vance, D., & Poulton, S. W. (2009). Mo isotope fractionation during adsorption to Fe (oxyhydr)oxides. *Geochimica et Cosmochimica Acta*, *73*(21), 6502–6516. <https://doi.org/10.1016/j.gca.2009.08.004>
- Goldberg, T., Archer, C., Vance, D., Thamdrup, B., McAnena, A., & Poulton, S. W. (2012). Controls on Mo isotope fractionations in a Mn-rich anoxic marine sediment, Gullmar Fjord, Sweden. *Chemical Geology*, *296–297*, 73–82. <https://doi.org/10.1016/j.chemgeo.2011.12.020>
- Goldberg, T., Poulton, S. W., Wagner, T., Kolonic, S. F., & Rehkämper, M. (2016). Molybdenum drawdown during Cretaceous oceanic anoxic event 2. *Earth and Planetary Science Letters*, *440*, 81–91. <https://doi.org/10.1016/j.epsl.2016.02.006>
- Gong, S., Hu, Y., Li, N., Feng, D., Liang, Q., Tong, H., et al. (2018). Environmental controls on sulfur isotopic compositions of sulfide minerals in seep carbonates from the South China Sea. *Journal of Asian Earth Sciences*, *168*, 96–105. <https://doi.org/10.1016/j.jseaes.2018.04.037>
- Gordon, G. W., Lyons, T. W., Arnold, G. L., Roe, J., Sageman, B. B., & Anbar, A. D. (2009). When do black shales tell molybdenum isotope tales? *Geology*, *37*(6), 535–538. <https://doi.org/10.1130/G25186A>
- Greber, N. D., Siebert, C., Nägler, T. F., & Pettke, T. (2012). $\delta^{98/95}\text{Mo}$ values and molybdenum concentration data for NIST SRM 610, 612 and 3134: Towards a common protocol for reporting Mo data. *Geostands and Geoanalytical Research*, *36*(3), 291–300. <https://doi.org/10.1111/j.1751-908X.2014.12047.x>
- Han, Y. M., Cao, J., Posmentier, E. S., Chow, J. C., Watson, J. G., Fung, K. K., et al. (2009). The effect of acidification on the determination of elemental carbon, char-and soot-elemental carbon in soils and sediments. *Chemosphere*, *75*(1), 92–99. <https://doi.org/10.1016/j.chemosphere.2008.11.044>
- He, Z., Clarkson, M. O., Andersen, M. B., Archer, C., Sweere, T. C., Kraal, P., et al. (2021). Temporally and spatially dynamic redox conditions on an upwelling margin: The impact on coupled sedimentary Mo and U isotope systematics, and implications for the Mo-U paleoredox proxy. *Geochimica et Cosmochimica Acta*, *309*, 251–271. <https://doi.org/10.1016/j.gca.2021.06.024>
- Helz, G., Miller, C., Charnock, J., Mosselmans, J., Patrick, R., Garner, C., & Vaughan, D. (1996). Mechanism of molybdenum removal from the Sea and its concentration in black shales: EXAFS evidence. *Geochimica et Cosmochimica Acta*, *60*(19), 3631–3642. [https://doi.org/10.1016/0016-7037\(96\)00195-0](https://doi.org/10.1016/0016-7037(96)00195-0)
- Helz, G. R., Bura-Nakić, E., Mikac, N., & Ciglenečki, I. (2011). New model for molybdenum behavior in euxinic waters. *Chemical Geology*, *284*(3–4), 323–332. <https://doi.org/10.1016/j.chemgeo.2011.03.012>
- Helz, G. R., & Vorlicek, T. P. (2019). Precipitation of molybdenum from euxinic waters and the role of organic matter. *Chemical Geology*, *509*, 178–193. <https://doi.org/10.1016/j.chemgeo.2019.02.001>
- Hu, Y., Chen, L., Feng, D., Liang, Q., Xia, Z., & Chen, D. (2017). Geochemical record of methane seepage in authigenic carbonates and surrounding host sediments: A case study from the South China Sea. *Journal of Asian Earth Sciences*, *138*, 51–61. <https://doi.org/10.1016/j.jseaes.2017.02.004>
- Hu, Y., Feng, D., Peckmann, J., Roberts, H. H., & Chen, D. (2014). New insights into cerium anomalies and mechanisms of trace metal enrichment in authigenic carbonate from hydrocarbon seeps. *Chemical Geology*, *381*, 55–66. <https://doi.org/10.1016/j.chemgeo.2014.05.014>
- Huang, H., Wang, X., Gong, S., Krake, N., Jin, M., Li, N., et al. (2020). New constraints on the formation of hydrocarbon-derived low magnesium calcite at brine seeps in the Gulf of Mexico. *Sedimentary Geology*, *398*, 105572. <https://doi.org/10.1016/j.sedgeo.2019.105572>
- Huang, T., Sun, X., Somelar, P., Kirsimäe, K., Pickering, R., Kim, J., et al. (2023). Separating Si phases from diagenetically-modified sediments through sequential leaching. *Chemical Geology*, *637*, 121681. <https://doi.org/10.1016/j.chemgeo.2023.121681>
- Hutchings, A. M., Basu, A., Dickson, A. J., & Turchyn, A. V. (2020). Molybdenum geochemistry in salt marsh pond sediments. *Geochimica et Cosmochimica Acta*, *284*, 75–91. <https://doi.org/10.1016/j.gca.2020.06.014>
- Jia, Z., Hu, Y., Bayon, G., Peckmann, J., Wang, X., Gong, S., et al. (2023a). Seawater-fluid composition records from molybdenum isotopes of sequentially extracted phases of seep carbonate rocks. *Geochemistry, Geophysics, Geosystems*, *24*(12), e2023GC011128. <https://doi.org/10.1029/2023GC011128>
- Jia, Z., Hu, Y., Bayon, G., Peckmann, J., Wang, X., Gong, S., et al. (2023b). Raw data for “molybdenum isotope fingerprinting of microbial sulfate reduction in seep carbonate rocks” [Dataset]. *Mendeley Data*, *V1*. Retrieved from <https://data.mendeley.com/datasets/25v8rtz9w5/1>
- Jørgensen, B. B. (2021). Sulfur biogeochemical cycle of marine sediments. *Geochemical Perspectives*, *10*, 145–307. <https://doi.org/10.7185/geochempersp.10.2>
- Joye, S. B., Boetius, A., Orcutt, B. N., Montoya, J. P., Schulz, H. N., Erickson, M. J., & Lugo, S. K. (2004). The anaerobic oxidation of methane and sulfate reduction in sediments from Gulf of Mexico cold seeps. *Chemical Geology*, *205*(3–4), 219–238. <https://doi.org/10.1016/j.chemgeo.2003.12.019>

- King, E. K., Perakis, S. S., & Pett-Ridge, J. C. (2018). Molybdenum isotope fractionation during adsorption to organic matter. *Geochimica et Cosmochimica Acta*, 222, 584–598. <https://doi.org/10.1016/j.gca.2017.11.014>
- LaRowe, D. E., Arndt, S., Bradley, J. A., Estes, E. R., Hoarfrost, A., Liang, S. Q., et al. (2020). The fate of organic carbon in marine sediments—New insights from recent data and analysis. *Earth-Science Reviews*, 204, 103146. <https://doi.org/10.1016/j.earscirev.2020.103146>
- Lee, D., Kim, J., Lee, J., Germain, B., Kim, D., Joe, Y., et al. (2022). Metalloenzyme signatures in authigenic carbonates from the Chukchi Borderlands in the western Arctic Ocean. *Scientific Reports*, 12(1), 16597. <https://doi.org/10.1038/s41598-022-21184-6>
- Li, J., Liang, X., Zhong, L., Wang, X., Ren, Z., Sun, S., et al. (2014). Measurement of the isotopic composition of molybdenum in geological samples by MC-ICP-MS using a novel chromatographic extraction technique. *Geostandards and Geoanalytical Research*, 38(3), 345–354. <https://doi.org/10.1111/j.1751-908X.2013.00279.x>
- Liang, Q., Hu, Y., Feng, D., Peckmann, J., Chen, L., Yang, S., et al. (2017). Authigenic carbonates from newly discovered active cold seeps on the northwestern slope of the South China Sea: Constraints on fluid sources, formation environments, and seepage dynamics. *Deep-Sea Research I*, 124, 31–41. <https://doi.org/10.1016/j.dsr.2017.04.015>
- Lin, Z., Sun, X., Strauss, H., Eroglu, S., Böttcher, M. E., Lu, Y., et al. (2021). Molybdenum isotope composition of seep carbonates—Constraints on sediment biogeochemistry in seepage environments. *Geochimica et Cosmochimica Acta*, 307, 56–71. <https://doi.org/10.1016/j.gca.2021.05.038>
- McLennan, S. M. (2001). Relationships between the trace element composition of sedimentary rocks and upper continental crust. *Geochemistry, Geophysics, Geosystems*, 2(4), 2000GC000109. <https://doi.org/10.1029/2000GC000109>
- Miller, C. A., Peucker-Ehrenbrink, B., Walker, B. D., & Franco, M. (2011). Re-assessing the surface cycling of molybdenum and rhenium. *Geochimica et Cosmochimica Acta*, 75(22), 7146–7179. <https://doi.org/10.1016/j.gca.2011.09.005>
- Naehr, T. H., Birgel, D., Bohrmann, G., MacDonald, I. R., & Kasten, S. (2009). Biogeochemical controls on authigenic carbonate formation at the Chapopote “asphalt volcano”, Bay of Campeche. *Chemical Geology*, 266(3–4), 390–402. <https://doi.org/10.1016/j.chemgeo.2009.07.002>
- Nägler, T. F., Anbar, A. D., Archer, C., Goldberg, T., Gordon, G. W., Greber, N. D., et al. (2014). Proposal for an international molybdenum isotope measurement standard and data representation. *Geostandards and Geoanalytical Research*, 38(2), 149–151. <https://doi.org/10.1111/j.1751-908X.2013.00275.x>
- Nägler, T. F., Neubert, N., Böttcher, M. E., Dellwig, O., & Schnetger, B. (2011). Molybdenum isotope fractionation in pelagic euxinia: Evidence from the modern Black and Baltic Seas. *Chemical Geology*, 289(1–2), 1–11. <https://doi.org/10.1016/j.chemgeo.2011.07.001>
- Nan, J., Tsang, M.-Y., Li, J., Köster, M., Henkel, S., Lin, F., & Yao, W. (2023). Postdepositional behavior of molybdenum in deep sediments and implications for paleoredox reconstruction. *Geophysical Research Letters*, 50(21), e2023GL104706. <https://doi.org/10.1029/2023GL104706>
- Neubert, N., Nægler, T. F., & Böttcher, M. E. (2008). Sulfidity controls molybdenum isotope fractionation into euxinic sediments: Evidence from the modern Black Sea. *Geology*, 36(10), 775–778. <https://doi.org/10.1130/G24959A.1>
- Osorio-Rodriguez, D., Metcalfe, K., McGlynn, S., Yu, H., Dekas, A., Ellisman, M., et al. (2023). Microbially induced precipitation of silica by anaerobic methane-oxidizing consortia and implications for microbial fossil preservation. *Proceedings of the National Academy of Sciences of the United States of America*, 120(51), e2302156120. <https://doi.org/10.1073/pnas.2302156120>
- O'Sullivan, E. M., Nægler, T. F., Turner, E. C., Kamber, B. S., Babechuk, M. G., & O'Hare, S. P. (2022). Mo isotope composition of the 0.85 Ga ocean from coupled carbonate and shale archives: Some implications for pre-Cryogenian oxygenation. *Precambrian Research*, 378, 106760. <https://doi.org/10.1016/j.precamres.2022.106760>
- Peckmann, J., & Thiel, V. (2004). Carbon cycling at ancient methane-seeps. *Chemical Geology*, 205(3–4), 443–467. <https://doi.org/10.1016/j.chemgeo.2003.12.025>
- Phillips, R., & Xu, J. (2021). A critical review of molybdenum sequestration mechanisms under euxinic conditions: Implications for the precision of molybdenum paleoredox proxies. *Earth-Science Reviews*, 221, 103799. <https://doi.org/10.1016/j.earscirev.2021.103799>
- Piper, D. Z., & Perkins, R. B. (2004). A modern vs. Permian black shale—the hydrography, primary productivity, and water-column chemistry of deposition. *Chemical Geology*, 206(3–4), 177–197. <https://doi.org/10.1016/j.chemgeo.2003.12.006>
- Poulson, R. L., Siebert, C., McManus, J., & Berelson, W. M. (2006). Authigenic molybdenum isotope signatures in marine sediments. *Geology*, 34(8), 617–620. <https://doi.org/10.1130/G22485.1>
- Poulton, S. W., Fralick, P. W., & Canfield, D. E. (2004). The transition to a sulphidic ocean 1.84 billion years ago. *Nature*, 431(7005), 173–177. <https://doi.org/10.1038/nature02912>
- Roberts, H. H., Feng, D., & Joye, S. B. (2010). Cold-seep carbonates of the middle and lower continental slope, northern Gulf of Mexico. *Deep-Sea Research II*, 57(21–23), 2040–2054. <https://doi.org/10.1016/j.dsr2.2010.09.003>
- Romaniello, S. J., Herrmann, A. D., & Anbar, A. D. (2016). Syndeositional diagenetic control of molybdenum isotope variations in carbonate sediments from the Bahamas. *Chemical Geology*, 438, 84–90. <https://doi.org/10.1016/j.chemgeo.2016.05.019>
- Rongemaille, E., Bayon, G., Pierre, C., Bollinger, C., Chu, N. C., Fouquet, Y., et al. (2011). Rare earth elements in cold seep carbonates from the Niger delta. *Chemical Geology*, 286(3–4), 196–206. <https://doi.org/10.1016/j.chemgeo.2011.05.001>
- Scholz, F., Siebert, C., Dale, A. W., & Frank, M. (2017). Intense molybdenum accumulation in sediments underneath a nitrogenous water column an implications for the reconstruction of paleo-redox conditions based on molybdenum isotopes. *Geochimica et Cosmochimica Acta*, 213, 400–417. <https://doi.org/10.1016/j.gca.2017.06.048>
- Siebert, C., Nægler, T. F., von Blanckenburg, F., & Kramers, J. D. (2003). Molybdenum isotope records as a potential new proxy for paleoceanography. *Earth and Planetary Science Letters*, 211(1–2), 159–171. [https://doi.org/10.1016/S0012-821X\(03\)00189-4](https://doi.org/10.1016/S0012-821X(03)00189-4)
- Smrzka, D., Feng, D., Himmler, T., Zwicker, J., Hu, Y., Monien, P., et al. (2020). Trace elements in methane-seep carbonates: Potentials, limitations, and perspectives. *Earth-Science Reviews*, 208, 103263. <https://doi.org/10.1016/j.earscirev.2020.103263>
- Smrzka, D., Zwicker, J., Misch, D., Walkner, C., Gier, S., Monien, P., et al. (2019). Oil seepage and carbonate formation: A case study from the southern Gulf of Mexico. *Sedimentology*, 66(6), 2318–2353. <https://doi.org/10.1111/sed.12593>
- Sun, Y., Feng, D., Smrzka, D., Peckmann, J., Huang, H., Roberts, H. H., & Chen, D. (2021). Uptake of trace elements into authigenic carbonate at a brine seep in the northern Gulf of Mexico. *Chemical Geology*, 582, 120442. <https://doi.org/10.1016/j.chemgeo.2021.120442>
- Sun, Y., Gong, S., Li, N., Peckmann, J., Jin, M., Roberts, H. H., et al. (2020). A new approach to discern the hydrocarbon sources (oil vs methane) of authigenic carbonates forming at marine seeps. *Marine and Petroleum Geology*, 114, 104230. <https://doi.org/10.1016/j.marpetgeo.2020.104230>
- Tessier, A., Campbell, P. G. C., & Bisson, M. (1979). Sequential extraction procedure for the speciation of particulate trace metals. *Analytical Chemistry*, 51(7), 844–851. <https://doi.org/10.1021/ac50043a017>
- Tong, H., Feng, D., Peckmann, J., Roberts, H. H., Chen, L., Bian, Y., & Chen, D. (2019). Environments favoring dolomite formation at cold seeps: A case study from the Gulf of Mexico. *Chemical Geology*, 518, 9–18. <https://doi.org/10.1016/j.chemgeo.2019.04.016>
- Tribouillard, N., Riboulleau, A., Lyons, T., & Baudin, F. (2004). Enhanced trapping of molybdenum by sulfurized marine organic of marine origin in Mesozoic limestones and shales. *Chemical Geology*, 213(4), 385–401. <https://doi.org/10.1016/j.chemgeo.2004.08.011>

- Vorlicek, T. P., Helz, G. R., Chappaz, A., Vue, P., Vezina, A., & Hunter, W. (2018). Molybdenum burial mechanism in sulfidic sediments: Iron-sulfide pathway. *ACS Earth and Space Chemistry*, 2(6), 565–576. <https://doi.org/10.1021/acsearthspacechem.8b00016>
- Wagner, M., Chappaz, A., & Lyons, T. W. (2017). Molybdenum speciation and burial pathway in weakly sulfidic environments: Insights from XAFS. *Geochimica et Cosmochimica Acta*, 206, 18–29. <https://doi.org/10.1016/j.gca.2017.02.018>
- Wang, X., Bayon, G., Kim, J.-H., Lee, D.-H., Kim, D., Guéguen, B., et al. (2019). Trace element systematics in cold seep carbonates and associated lipid compounds. *Chemical Geology*, 528, 119277. <https://doi.org/10.1016/j.chemgeo.2019.119277>
- Wasylenki, L. E., Rolfe, B. A., Weeks, C. L., Spiro, T. G., & Anbar, A. D. (2008). Experimental investigation of the effects of temperature and ionic strength on Mo isotope fractionation during adsorption to manganese oxides. *Geochimica et Cosmochimica Acta*, 72(24), 5997–6005. <https://doi.org/10.1016/j.gca.2008.08.027>
- Wegener, G., Niemann, H., Elvert, M., Hinrichs, K.-U., & Boetius, A. (2008). Assimilation of methane and inorganic carbon by microbial communities mediating the anaerobic oxidation of methane. *Environmental Microbiology*, 10(9), 2287–2298. <https://doi.org/10.1111/j.1462-2920.2008.01653.x>
- Zhao, P., Li, J., Zhang, L., Wang, Z., Kong, D., Ma, J., et al. (2016). Molybdenum mass fractions and isotopic compositions of international geological reference materials. *Geostandards and Geoanalytical Research*, 40(2), 217–226. <https://doi.org/10.1111/j.1751-908X.2015.00373.x>
- Zheng, Y., Anderson, R. F., Van Geen, A., & Kuwabara, J. (2000). Authigenic molybdenum formation in marine sediments: A link to pore water sulfide in the Santa Barbara Basin. *Geochimica et Cosmochimica Acta*, 64(24), 4165–4178. [https://doi.org/10.1016/S0016-7037\(00\)00495-6](https://doi.org/10.1016/S0016-7037(00)00495-6)